

Physics of collisionless phase mixing

D. Tsiklauri and T. Haruki

*Joule Physics Laboratory, Institute for Materials Research,
University of Salford, Manchester, M5 4WT, United Kingdom*

(Dated: November 9, 2018)

Previous studies of phase mixing of ion cyclotron (IC), Alfvénic, waves in the collisionless regime have established the generation of parallel electric field and hence acceleration of electrons in the regions of transverse density inhomogeneity. However, outstanding issues were left open. Here we use 2.5D, relativistic, fully electromagnetic PIC (Particle-In-Cell) code and an analytic MHD (Magnetohydrodynamic) formulation, to establish the following points: (i) Using the generalised Ohm's law we find that the parallel electric field is supported mostly by the electron pressure tensor, with a smaller contribution from the electron inertia term. (ii) The generated parallel electric field and the fraction of accelerated electrons are independent of the IC wave frequency remaining at a level of six orders of magnitude larger than the Dreicer value and approximately 20 % respectively. The generated parallel electric field and the fraction of accelerated electrons increase with the increase of IC wave amplitude. The generated parallel electric field seems to be independent of plasma beta, while the fraction of accelerated electrons strongly increases with the decrease of plasma beta (for plasma beta of 0.0001 the fraction of accelerated electrons can be as large as 47 %). (iii) In the collisionless regime IC wave dissipation length (that is defined as the distance over which the wave damps) variation with the driving frequency shows a deviation from the analytical MHD result, which we attribute to a possible frequency dependence of the effective resistivity. (iv) Effective anomalous resistivity, inferred from our numerical simulations, is at least four orders of magnitude larger than the classical Spitzer value.

PACS numbers: 52.35.Hr; 96.50.Tf; 04.30.Nk; 96.50.Ci; 96.60.P-; 52.65.Rr; 96.60.pf; 96.60.qe

I. INTRODUCTION

Phase mixing is a mechanism of enhanced dissipation of Alfvén waves due to inhomogeneity of Alfvén speed in a direction transverse to a local magnetic field. This mechanism originally was studied in the fusion and laboratory plasma context by a number of authors [1, 2, 3, 4, 5, 6] and subsequently applied to the solar corona [7]. Most of the large amount of work done in the field of phase mixing was in the resistive MHD (Magnetohydrodynamic) regime. Recently, a few works looked at the same mechanism in the collisionless regime in the context of Earth magnetosphere [8, 9] and solar corona [10, 11]. The main findings of these works include the generation of electric field that is parallel to the ambient magnetic field in the regions of transverse density inhomogeneity, as well as associated electron acceleration. It should be mentioned that these studies considered circularly polarised ion cyclotron (IC) waves which in the low frequency regime become Alfvén waves. We use terms Alfvén or IC interchangeably, but reader should bear in mind we always refer to *waves with frequencies* $< \omega_{ci}$ (with ω_{ci} being ion cyclotron frequency). The exact mechanism of generation of the parallel electric field has stimulated a debate [12, 13], and even MHD regime option was explored [14]. Continuing this investigation, here we apply technique used in the collisionless reconnection [15, 16]. Namely, in section 3.1 we use generalised Ohm's law to find out which term generates the parallel electric field.

Solar flare observations [17] trigger one's interest in how effectively plasma particles are accelerated. Hence, in section 3.2 we look into how the generated parallel

electric field and the fraction of accelerated electrons depend on model parameters such as IC wave frequency, amplitude, and plasma beta.

Ref. [7] provides a simple analytical expression how Alfvén wave amplitude should decay in space due to the phase mixing. Despite the fact that their formula is derived in the resistive MHD regime, we still apply it to our collisionless, kinetic simulation and see what does the comparison yield (Section 3.3). This is done in the light of previous results of Tsiklauri et al. [10] who established that in the collisionless, kinetic regime Alfvén wave amplitude in the density gradient regions decays with distance (from where it is driven) according to collisional MHD formula of Heyvaerts and Priest [7]. Here we stretch the MHD-kinetic analogy further to test ω_d^2 dependence under the exponent.

In Sect 3.4 we estimate the effective "resistivity" (again the spirit of MHD-kinetic analogy). The quotation marks are needed to signify that PIC (Particle-In-Cell) simulation code is collisionless and hence no resistive effects exist as such. However, scattering of particles by magnetic fields plays effective role of collisions.

II. SIMULATION MODEL

In our numerical simulations we use 2.5D, relativistic, fully electromagnetic PIC code. The initial conditions, basic parameters and boundary conditions are exactly the same as in the previous work by Tsiklauri et al. [10]. In particular, the uniform magnetic field is in x -direction, the transverse density inhomogeneity is across

y -direction. z is the spatially ignorable coordinate, i.e. $\partial/\partial z = 0$. However, we retain all three components of velocity, v_x , v_y and v_z . The system size without ghost cells in two dimensions is $L_x = 5000\Delta$ and $L_y = 200\Delta$ where $\Delta(= 1)$ is the simulation grid size, corresponding to the electron Debye length, $\lambda_D = v_{te}/\omega_{pe} = 1\Delta$ (v_{te} is electron thermal velocity and ω_{pe} is electron plasma frequency). The total particle number is 2.39×10^8 electron-ion pairs. The ion to electron mass ratio is $m_i/m_e = 16$ due to the limitation of computer resources and speed. Tsiklauri et al. [10] use the fixed driving wave amplitude $\delta B/B_0 = 0.05$, and plasma $\beta = 0.02$. The dimensionless ion and electron density inhomogeneity is described by

$$n_i(y) = n_e(y) = 1 + 3 \exp \left[- \left(\frac{y - 100\Delta}{50\Delta} \right)^6 \right] \equiv F(y).$$

These are normalised to some background constant value (n_0). Here all plasma parameters are quoted at the boundary, away from the density inhomogeneity region. In the central region (across y -coordinate), the density is smoothly enhanced by a factor of 4, and there are the strongest density gradients having a width of about 51Δ around the locations $y = 51.5\Delta$ and $y = 148.5\Delta$. Below, in Eqs.(4) and (5) we shall be using $y = 51.5 - 51/2 = 26\Delta$ and $y = 51.5 + 51/2 = 77\Delta$ as the boundaries of one of the transverse density gradients. The background temperature of ions and electrons, and their thermal velocities are varied accordingly

$$T_i(y)/T_0 = T_e(y)/T_0 = F(y)^{-1},$$

$$v_{th,i}/v_{i0} = v_{th,e}/v_{e0} = F(y)^{-1/2},$$

such that the thermal pressure remains constant. Since the background magnetic field along the x -coordinate is also constant, the total pressure remains constant too. Then we impose a current of the following form

$$\partial_t E_y = -J_0 \sin(\omega_d t) (1 - \exp[-(t/t_0)^2]),$$

$$\partial_t E_z = -J_0 \cos(\omega_d t) (1 - \exp[-(t/t_0)^2]).$$

In Ref. [10] the driving frequency was fixed at $\omega_d = 0.3\omega_{ci}$. Here, we also use driving frequencies that satisfy $\omega_d < \omega_{ci}$ so that no significant ion-cyclotron resonant damping takes place. ∂_t denotes the time derivative. t_0 is the onset time of the driver, which was fixed at $50/\omega_{pe}$ i.e. $3.125/\omega_{ci}$. This means that the driver onset time is about 3 ion-cyclotron periods. Imposing such a current on the system results in the generation of left circularly polarised IC (Alfvénic) wave, which is driven at the left boundary of simulation box and has spatial driver width of 1Δ . The wave propagates along x -coordinate and generates the parallel electric field in the density gradient regions (for more details see Tsiklauri et al. [10]). The parameters used are commensurate to what is seen in solar corona by e.g. Doppler broadening of emission lines.

The observed values of the Alfvén waves at heights of $R = 1.04R_{\text{sun}} = 28$ Mm are about 50 km s^{-1} (see e.g. [18]), which for a typical Alfvén speed of 1000 km s^{-1} makes $\delta B/B_0$ equal to 0.05.

As one of our goals is to investigate the parameter space of the problem, the following range of physical parameters was used: we vary the frequency, amplitude of IC wave or the plasma beta. The driving wave frequency ω_d/ω_{ci} ranged from 0.1 to 0.5 with a step of 0.1. The wave amplitude $\delta B/B_0$ was also set at 0.01, 0.05, 0.10, 0.15, 0.20 and 0.25. The plasma beta varies from $\beta = 10^{-4}$ to 10^{-2} by controlling the electron thermal velocity. Specifically, the plasma beta was set at 0.0001, 0.0003, 0.0010, 0.0030, 0.0100, 0.0200 and 0.0300. Each beta value corresponds to $v_{te}/c = 0.007, 0.012, 0.022, 0.039, 0.071, 0.100$ and 0.122 , respectively, where v_{te} is taken from the low density region and c is speed of light. Each numerical run (each data point in subsequent Figs. (2)-(5) typically takes about 7-10 days on 64 parallel processors.

III. SIMULATION RESULTS

A. Source of the parallel electric field

In order to understand details of the parallel electric field generation process, we now focus on the question: which term in the generalised Ohm's law is responsible for the generation of the parallel electric field? The generalised Ohm's law can be written as

$$\vec{E} = -\vec{v}_e \times \vec{B} - \frac{\nabla \cdot \vec{P}_e}{n_e e} - \frac{m_e}{e} \left(\frac{\partial \vec{v}_e}{\partial t} + (\vec{v}_e \cdot \nabla) \vec{v}_e \right), \quad (1)$$

where \vec{E} and \vec{B} are electric and magnetic fields, \vec{v} is plasma velocity, \vec{P} is pressure tensor (3×3 matrix), n is plasma number density, m is mass and e is electric charge. The subscript e refers to an electron. Normalising space coordinate by $L_x = 5000\Delta$, fluid velocity by Alfvén speed (at the lowest density region) v_{A0} , time by Alfvén transit time $\tau_A (= L/v_{A0})$, magnetic field by B_0 , electric field by $v_{A0}B_0$, number density by n_0 and pressure tensor by B_0^2/μ_0 , a dimensionless version of Eq. (1) can be obtained

$$\vec{E} = -\vec{v}_e \times \vec{B} - d_i \frac{\nabla \cdot \vec{P}_e}{n_e} - d_i \frac{m_e}{m_i} \left(\frac{\partial \vec{v}_e}{\partial t} + (\vec{v}_e \cdot \nabla) \vec{v}_e \right), \quad (2)$$

where d_i is the normalised ion skin depth ($d_i = c/\omega_{pi}L$). Note that strictly speaking we should have used tildes in Eq. (2) to denote dimensionless quantities, but we omit them for brevity.

Let us focus on the parallel electric field, E_x , which is generated in the density gradient regions by phase mix-

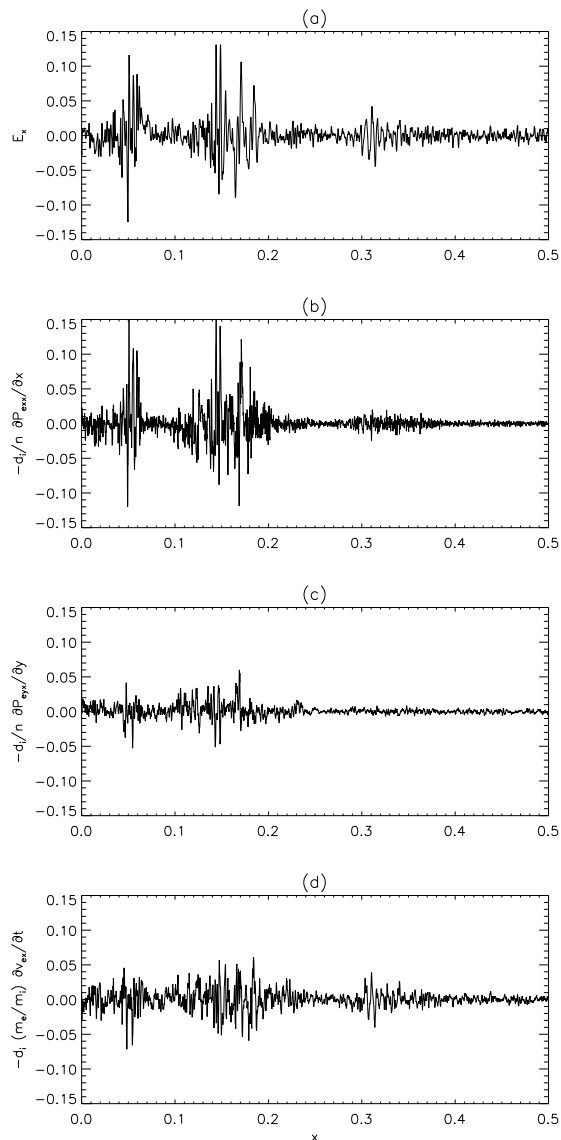


FIG. 1: Different term profiles along x -coordinate from the generalised Ohm's law: (a) E_x (normalised to $v_{A0}B_0$), (b) $-(d_i/n)\partial P_{exx}/\partial x$, (c) $-(d_i/n)\partial P_{eyx}/\partial y$, and (d) $-d_i(m_e/m_i)\partial v_{ex}/\partial t$ in the maximum density gradient region $y = 0.0103$ at $t = 0.4375$ for the case, $\omega_d/\omega_{ci} = 0.3$, $\delta B/B_0 = 0.25$ and $\beta = 0.02$. The time derivative term in (d) is calculated from $t = 0.4370$ to 0.4375 (time interval corresponds to the inverse of electron plasma frequency ω_{pe}^{-1}). Refer to text for the normalisation used.

ing. It is given by,

$$E_x = -(v_{ey}B_z - v_{ez}B_y) - d_i \frac{1}{n} \left(\frac{\partial P_{exx}}{\partial x} + \frac{\partial P_{eyx}}{\partial y} \right) - d_i \frac{m_e}{m_i} \left(\frac{\partial v_{ex}}{\partial t} + v_{ex} \frac{\partial v_{ex}}{\partial x} + v_{ey} \frac{\partial v_{ex}}{\partial y} \right), \quad (3)$$

where $\partial/\partial z = 0$ is assumed because of spatially 2 dimensional model.

Fig. 1 shows the different term profiles (along the uni-

form magnetic field in x -direction) in the generalised Ohm's law (Eq. (3)): (a) E_x , (b) $-(d_i/n)\partial P_{exx}/\partial x$, (c) $-(d_i/n)\partial P_{eyx}/\partial y$, and (d) $-d_i(m_e/m_i)\partial v_{ex}/\partial t$ in the maximum density gradient region $y = 0.0103$ at $t = 0.4375$ for the case, $\omega_d/\omega_{ci} = 0.3$, $\delta B/B_0 = 0.25$ and $\beta = 0.02$. The time derivative term in Fig. 1(d) is calculated from $t = 0.4370$ to 0.4375 (time interval corresponds to the inverse of electron plasma frequency ω_{pe}^{-1}). The other terms in right-hand side of Eq. (3) are negligible. In Fig. 1(a), the parallel electric field is clearly observed in the density gradient regions where phase mixing can occur. It should be noted that no parallel electric field is seen away from the density gradient regions. According to the generalised Ohm's law, there has to be a term on the right-hand side of Eq. (3) that supports this electric field.

By comparing Fig. 1(a) to Fig. 1(b-d) it is clear that the parallel electric field (Fig. 1(a)) is supported mostly by the electron pressure tensor (Fig. 1(b)), with a smaller contribution from the electron inertia term (Fig. 1(d)). It is interesting to note that previous results on collisionless reconnection both in tearing unstable Harris current sheet [15, 19, 20] and stressed X-point collapse [16, 21] have shown that the term in the generalised Ohm's law that is responsible for breaking the frozen-in condition, i.e. that supports out-of-plane electric field is electron pressure tensor. Here the electron pressure tensor supports (generates) the parallel electric field. Thus, one should note a universal importance of the electron pressure tensor in relation to supporting the electric fields in collisionless plasmas.

B. Parametric study of the generated parallel electric field and the fraction of accelerated electrons

To estimate how efficiently the parallel electric field is generated by phase mixing, as a function of model parameters, we introduce the average of the absolute value of the parallel electric field in the density gradient region:

$$\frac{E^*}{E_0} = \frac{1}{L_x L_y} \int_{x=0}^{L_x} \int_{y=26\Delta}^{77\Delta} \frac{|E_x(x, y)|}{E_0} dx dy, \quad (4)$$

where $E_0 = m_e c \omega_{pe} / e$. Note that in what follows the normalisation of the electric field is different from Section 3.1 where, usual for the generalised Ohm's law, "fluid" normalisation ($v_{A0}B_0$) is used. Normalisation $E_0 = m_e c \omega_{pe} / e$ is usually referred to as "electrostatic". By using the definition given by Eq.(4) we can evaluate quantitatively the electric field generated in the density gradient region. Although there are two density regions in our simulation box because of the periodic boundary condition, we focus on the lower one (the physics of the upper and the lower regions is essentially the same). The range from $y = 26\Delta$ to 77Δ indicates the density gradient. See Tsiklauri et al. [10] for details.

Also, in order to investigate the fraction of accelerated electrons by the generated parallel electric field,

we use particle data in the density gradient at lower side ($26\Delta \leq y \leq 77\Delta$). We count the number of electrons with velocities greater than the thermal velocity ($v_{te} < v_x < c$) in the electron velocity distribution function, in the x -direction, at the final time snapshot $\omega_{ci}t = 54.69$, and divide this by the total number of particles (with $0 < v_x < c$) in the same domain:

$$\frac{N}{N_0} = \frac{\int_{v_x=v_{te}}^c \int_{x=0}^{L_x} \int_{y=26\Delta}^{77\Delta} f(v_x) dv_x dx dy}{\int_{v_x=0}^c \int_{x=0}^{L_x} \int_{y=26\Delta}^{77\Delta} f(v_x) dv_x dx dy}. \quad (5)$$

Here it was to enough to integrate only positive region in this distribution because electron acceleration was symmetrical in the x -direction. Note that the initial velocity distribution function is nearly Maxwellian. To maintain the balance of the total kinetic pressure throughout the system, the particle thermal velocity in the dense plasma region ($y = 100\Delta$) is lower than the outside region ($y = 0\Delta$ or 200Δ) (see for details Fig.(4) from Tsiklauri et al. [10]). However, in order to use Eq. (5), we had to estimate an appropriate velocity corresponding to the thermal velocity in the Maxwellian. Fortunately, initial electron velocity distribution function did not deviate much from the exact Maxwellian. Therefore, we adopted the standard thermal velocity which was set to 36.8% of $f(v = 0)$. Recall that $f(v = v_{te}) = n_0 \exp(-v^2/v_{te}^2) = n_0 \exp(-1.0) = 0.368n_0$, where n_0 is the peak number at $v = 0$ in Maxwellian.

The choice of diagnostic for characterizing the degree of particle acceleration needs a further clarification. Eq.(5) provides number of electrons with speed v_x exceeding the thermal speed v_{te} as a fraction of total distribution value. However, in a Maxwellian plasma 16% of the electrons have $v > v_{te}$ (for $v_{te} = \sqrt{2k_B T_e/m_e}$). Thus, it may be tempting to either: (i) subtract this 16% from our diagnostic in Eq.(5) or (ii) try to fit a Maxwellian to the electron distribution at the final simulation time step (after all the acceleration has taken place) and then count the number of electrons that have speeds $v_x > v_{te}$. Our motivation to keep the definition given by Eq.(5) is two-fold: (i) In context of the solar flare observations in X-rays, one always infers the integrated spectrum averaged over some volume V , i.e. $\langle f(v)nV \rangle$ (where n is electron number density) and it is impossible to subtract the above mentioned 16% without introducing additional uncertainties due to the unknown density and poorly known emitting volume, due to a line of sight effect (Dr. E. Kontar of University of Glasgow, private communication), see also Refs. [22, 23]. Hence the definition given by Eq.(5) is more appropriate for comparison of theory with the observations. Also, this is particularly timely because the acceleration of electrons by Alfvénic waves in flares have been recently studied [24]. (ii) Although the electron distribution function at the initial time step is nearly Maxwellian (despite density and temperature transverse inhomogeneities), at the final stages of the simulation the deviations from the Maxwellian form are large and hence a fit to a Maxwellian, in order

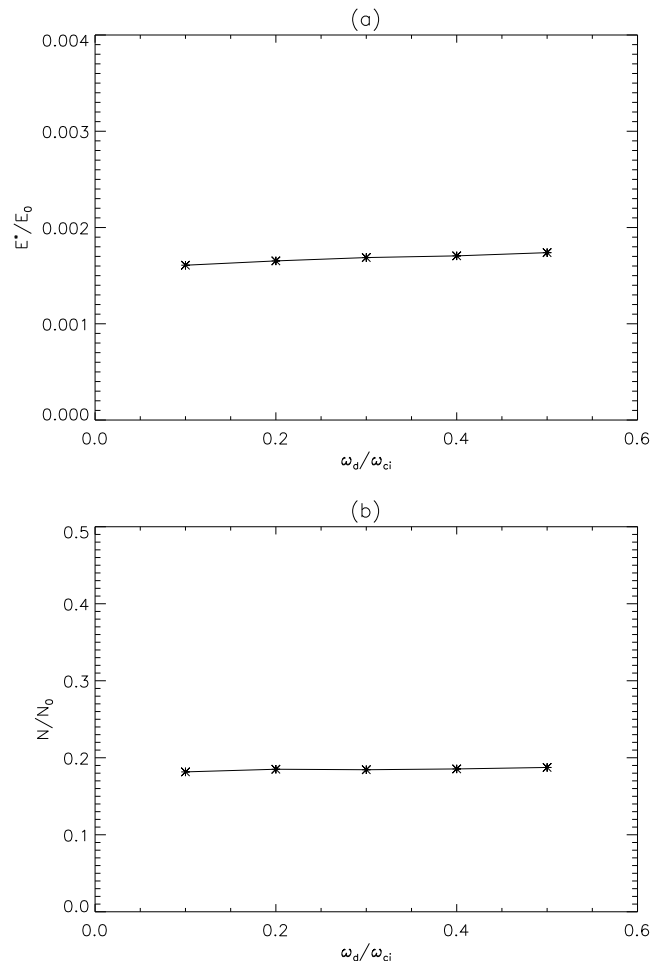


FIG. 2: (a) E^*/E_0 vs. ω_d/ω_{ci} and (b) N/N_0 vs. ω_d/ω_{ci} for $\delta B/B_0 = 0.05$ and $\beta = 0.02$.

to calculate v_{te} , and in turn to count the super-thermal particles above that value ($v_x > v_{te}$), is impractical.

Fig. (2) shows the generated parallel electric field, E^*/E_0 , and the fraction of accelerated electrons, N/N_0 as function of driving frequency of the IC wave (normalised to ω_{ci}). The wave frequency ω_d/ω_{ci} was set at 0.1, 0.2, 0.3, 0.4 and 0.5. The wave amplitude and plasma beta were fixed at $\delta B/B_0 = 0.05$ and $\beta = 0.02$. We gather from Fig. (2) that the generated parallel electric field and the fraction of accelerated electrons are independent of the IC wave frequency remaining at a level of six orders of magnitude larger than the Dreicer value and approximately 20 % respectively. This conclusion is based on the following estimate $E^*/E_0 \approx 0.0018$, i.e. $E^* = 5473.4337 \text{ V m}^{-1}$ (note that here solar coronal number density of $n = 10^{15} \text{ m}^{-3}$ was used). The Dreicer electric field (which is associated with the particle acceleration run-away regime [25]), $E_d = (ne^3 \ln \Lambda)/(4\pi\epsilon_0^2 k_B T)$, for $T = 1 \text{ MK}$ (and hence $\ln \Lambda = 18.095$) is $E_d = 0.00547 \text{ V}$

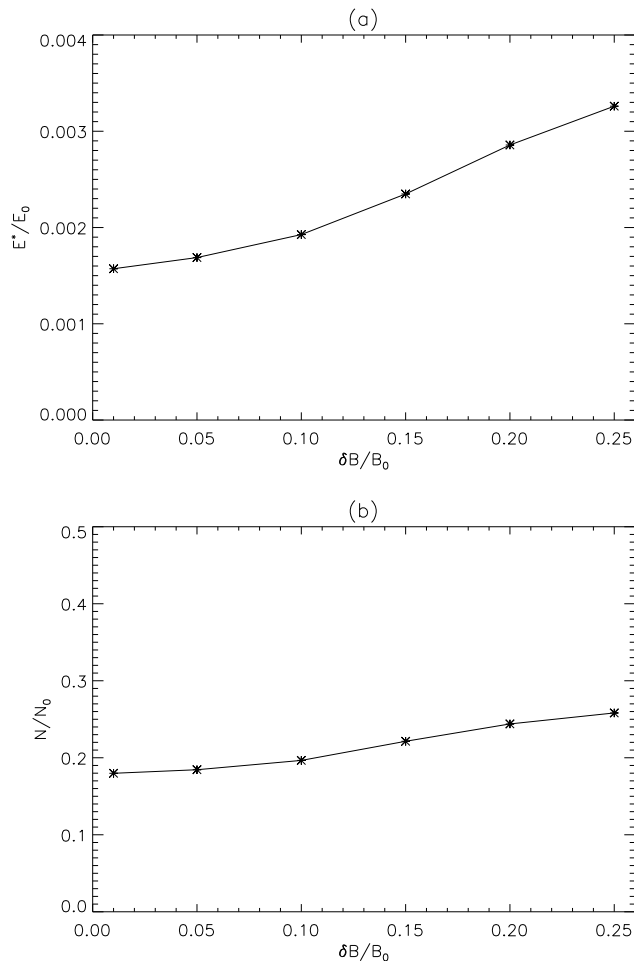


FIG. 3: (a) E^*/E_0 vs. $\delta B/B_0$ and (b) N/N_0 vs. $\delta B/B_0$ for $\omega_d/\omega_{ci} = 0.3$ and $\beta = 0.02$.

m^{-1} . Thus, $E^*/E_d = 10^6$. This result should be taken with caution because it is obtained with the ion-electron mass ratio of 16. As shown by Tsiklauri [13] (see their Figure 7) that attained amplitude of the generated parallel electric field scales strongly as $\propto 1/(m_i/m_e)$.

Next, we explore how the generated parallel electric field and the fraction of accelerated electrons depend on driving IC wave amplitude. The latter, $\delta B/B_0$, was set at 0.01, 0.05, 0.10, 0.15, 0.20 and 0.25. The wave frequency and plasma beta were fixed at $\omega_d/\omega_{ci} = 0.3$ and $\beta = 0.02$. We gather from Fig. 3 that the generated parallel electric field and the fraction of accelerated electrons increase with the increase of IC wave amplitude. This seems as a reasonable result because larger amplitude waves have more energy to give to electrons. Also, non-linear effects would be progressively important.

We also explored the plasma beta dependence. The plasma beta was set at 0.0001, 0.0003, 0.0010, 0.0030, 0.0100, 0.0200 and 0.0300.

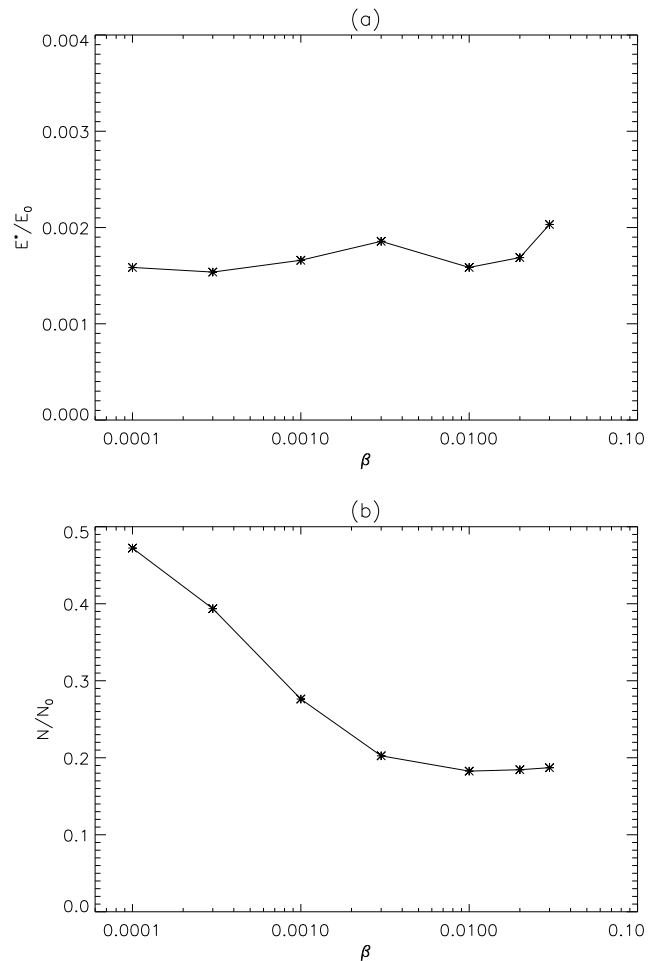


FIG. 4: (a) E^*/E_0 vs. β and (b) N/N_0 vs. β for $\omega_d/\omega_{ci} = 0.3$ and $\delta B/B_0 = 0.05$.

The wave frequency and amplitude were fixed at $\omega_d/\omega_{ci} = 0.3$ and $\delta B/B_0 = 0.05$. The plasma beta is defined as $\beta = 2\mu_0 p/B^2 = 2(v_{te}/c)^2/(\omega_{ce}/\omega_{pe})^2$. We altered the plasma beta by changing the electron thermal velocity, affecting the plasma kinetic pressure. Therefore, in this simulation, magnetic pressure is kept constant while plasma kinetic pressure varies. Fig. 4(a) does not show any correlation between plasma beta and the parallel electric field generation. Incidentally, Tsiklauri et al. [26] investigated plasma beta dependence of the fast magnetosonic wave amplitude, which is generated in a transversely inhomogeneous medium when an Alfvénic pulse is launched (using MHD numerical simulation). According to Fig. 9(b) in Tsiklauri et al. [26], the maximum fast magnetosonic wave amplitude also does not depend on plasma beta. Tsiklauri [14] alluded to the relation between the non-linear fast magnetosonic wave and parallel electric field generation. Hence it is not surprising that in our Fig. 4(a) we do

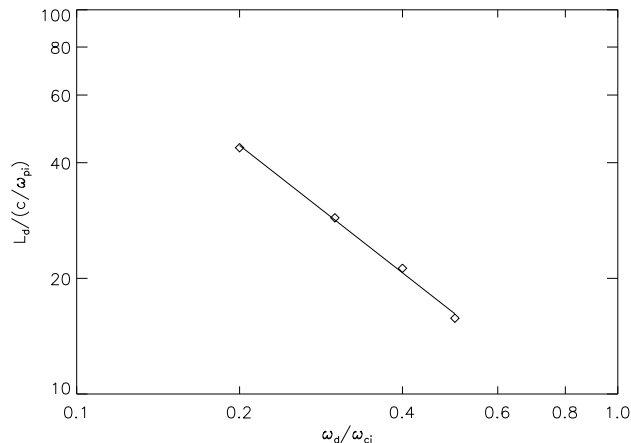


FIG. 5: A log-log plot of the dissipation length $L_d/(c/\omega_{pi})$ vs. driving IC wave frequency ω_d/ω_{ci} (open symbols). The solid line is the least squares fit with a slope of -1.10 .

not see plasma beta dependence. What is surprising, at the first glance, in Fig. 4(b), is that the fraction of accelerated particles strongly depends on beta. In particular, a decrease in beta (for $\beta = 0.0001$) yields as large percentage as $N/N_0 = 0.472 \sim 47\%$! One can conjecture that this is due to the fact that in the case of small plasma beta, magnetic effects dominate over thermal ones, and because IC wave is essentially a magnetic-type perturbation, electrons respond better to the wave influence and accelerate more efficiently.

C. Amplitude decay law in the kinetic regime

Tsiklauri et al. [10] established that in the collisionless, kinetic regime Alfvén (IC) wave amplitude in density gradient region decays with distance (from where it is driven) according to collisional MHD formula of Heyvaerts and Priest [7]

$$B_z \sim \exp \left[-\frac{\eta \omega_d^2 (\partial_y v_A)^2}{6v_A^5} x^3 \right], \quad (6)$$

where η is resistivity (divided by μ_0 , i.e. by η we mean $1/(\sigma\mu_0)$), ω_d is (driving) wave frequency, v_A is Alfvén velocity and x is the axis which AW propagates. Recall that plasma density inhomogeneity is a function of y and wave propagates in the x direction. In particular, (see for details left panel of Fig.6 in Tsiklauri et al. [10]) it was shown that, at a fixed time instance corresponding to well-developed phase mixing, $B_z(x) \propto \exp(-x/L_d)^3$. In other words, one can define an empirical dissipation length, L_d , according to collisional MHD formula (Eq.(6)) in the collisionless, kinetic regime. Applicability of the MHD formula in the kinetic regime was rather surprising. We now turn back to the previous results in order to see how far this MHD-kinetic analogy can be stretched.

In particular, one can e.g. check the ω_d^2 scaling in the Eq.(6). For this purpose, after simple algebra applied to $B_z \propto \exp[-(x/L_d)^3]$, for fixed η , $\partial_y v_A$ and v_A , one can obtain the following scaling $\log_{10} L_d = -2/3 \log_{10} \omega_d + C$, where C is some constant. Hence the slope of a log-log graph of dissipation length L_d versus ω_d is expected to be $-2/3 = -0.67$. Fig. 5 presents the dissipation length (distance over which the wave damps) dependence on the IC wave frequency. The values in Fig. 5 were obtained from line data of magnetic field B_z in the maximum plasma gradient $Y/(c/\omega_{pe}) = 14.8$ at $\omega_{ci}t = 82.0$ for $\omega_d/\omega_{ci} = 0.2$, $\omega_{ci}t = 54.7$ for $\omega_d/\omega_{ci} = 0.3$, $\omega_{ci}t = 41.0$ for $\omega_d/\omega_{ci} = 0.4$ and $\omega_{ci}t = 32.8$ for $\omega_d/\omega_{ci} = 0.5$, respectively. The reason for the different snapshot times is that we only consider well-developed phase mixing, i.e. when IC wave is fully damped. As in left panel of Fig.6 in Tsiklauri et al. [10] we fit $B_z(x)$ to $\propto \exp(-(x/L_d)^3)$ and obtain empirical dissipation length L_d . We gather from Fig. 5 that the slope is -1.10 contrary to the above prediction of $-2/3 = -0.67$.

To address the inconsistency we conjecture that the resistivity might be variable. One can estimate the resistivity for each case of driving wave frequency considered, by calculating $\eta = 6v_A^5/(\omega_d^2(\partial_y v_A)^2 L_d^3)$. We reiterate that strictly speaking PIC simulation code is collisionless and hence no resistive effects exist. However, scattering of particles by magnetic fields plays effective role of collisions. When resistivity is mentioned we refer to "effective" resistivity. Normalising the frequency by IC frequency ω_{ci} , length by ion skin depth c/ω_{pi} and velocity by speed of light c , the dimensionless resistivity is given by,

$$\frac{\eta}{c^2 \omega_{pi} / \omega_{ci}^2} = \frac{2}{27} \left(\frac{\omega_d}{\omega_{ci}} \right)^{-2} \left(\frac{L}{c/\omega_{pi}} \right)^2 \left(\frac{L_d}{c/\omega_{pi}} \right)^{-3} \left(\frac{v_A}{c} \right)^3 \sqrt{1 + 3 \exp \left[-\left(\frac{y - y_c}{L} \right)^6 \right]} \exp \left[2 \left(\frac{y - y_c}{L} \right)^6 \right] \left(\frac{y - y_c}{L} \right)^{-10}. \quad (7)$$

We can now put in the known parameters $L/(c/\omega_{pi}) = 1.25$, $v_A/c = 0.25$ and $(y - y_c)/L = (148.5 - 100)/50 = 0.97$ into Eq. (7). Here L and y_c are the width and the centre of plasma density gradient, respectively. Therefore the dimensionless resistivity can be estimated using

$$\frac{\eta}{c^2 \omega_{pi} / \omega_{ci}^2} = 1.97 \times 10^{-2} \left(\frac{\omega_d}{\omega_{ci}} \right)^{-2} \left(\frac{L_d}{c/\omega_{pi}} \right)^{-3}. \quad (8)$$

As the driving wave frequency and the dissipation length for each case are given by choice and empirically, respectively, one can obtain the resistivity by substituting above values into Eq. (8). The result is $\eta/(c^2 \omega_{pi} / \omega_{ci}^2) = 5.88 \times 10^{-6}$ (for $\omega_d/\omega_{ci} = 0.2$), 9.21×10^{-6} (for $\omega_d/\omega_{ci} = 0.3$), 1.28×10^{-5} (for $\omega_d/\omega_{ci} = 0.4$) and 2.02×10^{-5} (for $\omega_d/\omega_{ci} = 0.5$). Thus our initial conjecture that the

effective resistivity depends on the driving IC wave frequency turns out to be correct. But the main conclusion of this analysis is that despite collisional MHD scaling Eq.(6) being applicable to the collisionless, kinetic regime of phase mixing, i.e. $B_z(x) \propto \exp(-(x/L_d)^3)$ scaling holds, stretching the MHD-kinetic analogy further to ω_d^2 dependence under the exponent is not valid (due to the effective resistivity being a function of ω_d).

D. Effective anomalous resistivity

Issue of anomalous resistivity is central for many space and laboratory plasma applications. It can facilitate fast magnetic reconnection via Petschek type mechanism (if η is not spatially uniform), or have significant implications for wave heating models of solar corona where normal Spitzer resistivity is too small to produce any sizable effect. Ref.[27] presented plasma resistivity measurements in the reconnection current sheet of Magnetic Reconnection Experiment (MRX) (see ref.[28] for details of the experimental setup). They established that in the collisionless regime measured resistivity values can be more than an order of magnitude larger than the Spitzer value [27].

Let us apply our PIC simulation results to see if there is any evidence for the anomalous effective resistivity. We fix physical parameters corresponding to solar coronal plasmas: $B = 0.01T$ and plasma number density $n_0 = 2 \times 10^{15} m^{-3}$, i.e. $\omega_{ci} = eB/(16m_e) = 1.10 \times 10^8 rad/s$ and $\omega_{pi} = \sqrt{n_0 e^2 / (16m_e \epsilon_0)} = 6.30 \times 10^8 rad/s$. Eq. (8) can be rewritten as:

$$\eta = 9.24 \times 10^7 \left(\frac{\omega_d}{\omega_{ci}} \right)^{-2} \left(\frac{L_d}{c/\omega_{pi}} \right)^{-3}. \quad (9)$$

Similarly to the previous calculation in Eq. (8), now using Eq. (9) we obtain $\eta = 2.76 \times 10^4$ (for $\omega_d/\omega_{ci} = 0.2$), 4.32×10^4 (for $\omega_d/\omega_{ci} = 0.3$), 6.02×10^4 (for $\omega_d/\omega_{ci} = 0.4$) and 9.46×10^4 (for $\omega_d/\omega_{ci} = 0.5$). Here units of the resistivity are $m^2 sec^{-1}$. We gather that all values are in the range of $\approx 10^4 - 10^5 m^2 sec^{-1}$. Spitzer resistivity (normalised to μ_0) for the above parameters and $T = 1$ MK is $1.83 m^2 sec^{-1}$. Thus, we conclude that our numerical simulations provide effective resistivity values of $\approx 10^4$ times larger than Spitzer value, which is indicative of the anomalous resistivity. It should be mentioned that these results were obtained for the ion-to-electron mass ratio of 16. Clearly one would expect some dependence of the obtained effective resistivity on the mass ratio. Thus, the obtained results should be taken with caution.

IV. CONCLUSIONS

Let us summarise the above findings:

We used the generalised Ohm's law and found that the parallel electric field, which is generated by propagation of IC (Alfvénic) wave in a transversely inhomogeneous plasma, is supported mostly by the electron pressure tensor, with a smaller contribution from the electron inertia term. Surprisingly, this result resembles closely to the previous results on collisionless reconnection both in tearing unstable Harris current sheet [15, 19, 20] and stressed X-point collapse [16, 21]. However, in the latter two cases, the generated electric field is in the plane perpendicular to the magnetic field. Thus, a universal importance of the electron pressure tensor in relation to supporting the electric fields in collisionless plasmas should be noted.

We explored physical parameter space of the problem with regards to the efficiency of generation of parallel electric field and acceleration of electrons. We found that the generated parallel electric field and the fraction of accelerated electrons are independent of the IC wave frequency staying at a level that is 10^6 times larger than the Dreicer value and approximately 20 % respectively. The generated parallel electric field and the fraction of accelerated electrons increase with the increase of IC wave amplitude. The generated parallel electric field seems to be independent of plasma- β . However, the fraction of accelerated electrons strongly increases with the decrease of plasma- β , e.g. for plasma $\beta = 0.0001$ the fraction of accelerated electrons can be as large as 47 %.

Previously it was established that in the collisionless, kinetic regime phase-mixed Alfvén (IC) wave amplitude damps with distance of propagation according to $\propto \exp[-(x/L_d)^3]$ [10], which resembles closely to collisional MHD result of Heyvaerts and Priest [7]. We tried to stretch this analogy further by investigating how the dissipation length L_d scales with the IC driving frequency. We found that the scaling is different from the MHD result. We have shown that this discrepancy can be attributed to the frequency dependence of the effective resistivity.

We also found that the effective resistivity, albeit for unrealistic mass ratio, still is as large as 10^4 times the classical Spitzer value.

Acknowledgments

Numerical calculations of this work were performed using the MHD Cluster at University of St Andrews. Author acknowledges useful discussion of solar flare observational aspects with Dr. E. Kontar. This research was supported by the United Kingdom's Science and Technology Facilities Council (STFC).

-
- [1] C. Uberoi, Phys. Fluids **15**, 1673 (1972).
- [2] J. Tataronis and W. Grossmann, Zeitschrift fur Physik **261**, 203 (1973).
- [3] W. Grossmann and J. Tataronis, Zeitschrift fur Physik **261**, 217 (1973).
- [4] A. Hasegawa and L. Chen, Phys. Rev. Lett. **32**, 454 (1974).
- [5] L. Chen and A. Hasegawa, Phys. Fluids **17**, 1399 (1974).
- [6] J. A. Tataronis, J. Plasma Phys. **13**, 87 (1975).
- [7] J. Heyvaerts and E. R. Priest, Astron. Astrophys. **117**, 220 (1983).
- [8] V. Génot, P. Louarn, and D. Le Quéau, J. Geophys. Res. **104**, 22649 (1999).
- [9] V. Génot, P. Louarn, and F. Mottez, Ann. Geophysicae **22**, 2081 (2004).
- [10] D. Tsiklauri, J.-I. Sakai, and S. Saito, Astron. Astrophys. **435**, 1105 (2005).
- [11] D. Tsiklauri, J.-I. Sakai, and S. Saito, New J. Physics **7**, 79 (2005).
- [12] F. Mottez, V. Génot, and P. Louarn, Astron. Astrophys. **449**, 449 (2006).
- [13] D. Tsiklauri, New J. Physics **9**, 262 (2007).
- [14] D. Tsiklauri, Astron. Astrophys. **455**, 1073 (2006).
- [15] P. L. Pritchett, J. Geophys. Res. **106**, 3783 (2001).
- [16] D. Tsiklauri and T. Haruki, "Physics of collisionless reconnection in a stressed X-point collapse", Physics of Plasmas (in press) (2008).
- [17] L. Fletcher, Space Science Reviews **121**, 141 (2005).
- [18] T. G. Moran, Astron. Astrophys. **374**, L9 (2001).
- [19] M. Hesse, K. Schindler, J. Birn, and M. Kuznetsova, Phys. Plasmas **6**, 1781 (1999).
- [20] J. Birn, J. F. Drake, M. A. Shay, B. N. Rogers, R. E. Denton, M. Hesse, M. Kuznetsova, Z. W. Ma, A. Bhattacharjee, A. Otto, J. Geophys. Res. **106**, 3715 (2001).
- [21] D. Tsiklauri and T. Haruki, Phys. Plasmas **14**, 112905 (2007).
- [22] J. C. Brown, A. G. Emslie, and E. P. Kontar, Astrophys. J. **595**, L115 (2003).
- [23] J. C. Brown and E. P. Kontar, Adv. Space Res. **35**, 1675 (2005).
- [24] L. Fletcher and H. S. Hudson, Astrophys. J. **675**, 1645 (2008).
- [25] H. Dreicer, Phys. Rev. **115**, 238 (1959).
- [26] D. Tsiklauri, V. M. Nakariakov, and T. D. Arber, Astron. Astrophys. **395**, 285 (2002).
- [27] F. Trintchouk, M. Yamada, H. Ji, R. M. Kulsrud, and T. A. Carter, Phys. Plasmas **10**, 319 (2003).
- [28] M. Yamada, H. Ji, S. Hsu, T. Carter, R. Kulsrud, N. Bretz, F. Jobes, Y. Ono, and F. Perkins, Phys. Plasmas **4**, 1936 (1997).